Geomechanics and Engineering, *Vol. 14, No. 4 (2018) 337-344*
DOI: https://doi.org/10.12989/gae.2018.14.4.337

Numerical simulation on mining effect influenced by a normal fault and its induced effect on rock burst

Jin-Quan Jiang[1a], Pu Wang [*1], Li-Shuai Jiang[**2], Peng-Qiang Zheng[3b] and Fan Feng[4c]

[1]*State Key Laboratory of Mining Disaster Prevention and Control Co-founded by Shandong Province and the Ministry of Science and Technology, Shandong University of Science and Technology, Qingdao, China*
[2]*School of Mining and Safety Engineering, Shandong University of Science and Technology, Qingdao, China*
[3]*Department of Resources and Civil Engineering, Shandong University of Science and Technology, Tai'an China*
[4]*School of Resources and Safety Engineering, Central South University, Changsha, China*

(Received June 26, 2016, Revised July 12, 2017, Accepted August 7, 2017)

Abstract. The study of the mining effect influenced by a normal fault has great significance concerning the prediction and prevention of fault rock burst. According to the occurrence condition of a normal fault, the stress evolution of the working face and fault plane, the movement characteristics of overlying strata, and the law of fault slipping when the working face advances from footwall to hanging wall are studied utilizing UDEC numerical simulation. Then the inducing-mechanism of fault rock burst is revealed. Results show that in pre-mining, the in situ stress distribution of two fault walls in the fault-affected zone is notably different. When the working face mines in the footwall, the abutment stress distributes in a "double peak" pattern. The ratio of shear stress to normal stress and the fault slipping have the obvious spatial and temporal characteristics because they vary gradually from the higher layer to the lower one orderly. The variation of roof subsidence is in S-shape which includes slow deformation, violent slipping, deformation induced by the hanging wall strata rotation, and movement stability. The simulation results are verified via several engineering cases of fault rock burst. Moreover, it can provide a reference for prevention and control of rock burst in a fault-affected zone under similar conditions.

Keywords: normal fault; mining-induced stress; fault slipping; rock burst

1. Introduction

Owing to the increased amount of coal mining and depth of mining activities, geological conditions are becoming gradually more and more complex in East China, North China, Central China and Southwest China (Yong *et al.* 2015, Fan *et al.* 2017). Dynamic disasters such as coal and gas outburst, rock burst, and shock bump are induced because of the complex geological conditions. Therein, fault is the larger-affected and common-caused geological structure. Fault modifies the continuity of the rock masses and causes the singularities of the mining effect (Jiang *et al.* 2014). It might easily cause serious dynamic disasters. Fig. 1 shows several on-site images after two rock burst accidents induced by the fault marked as SF28 in Jining No. 3 coalmine (2004) and the fault marked as F16 in Qianqiu coalmine (2011).

Mining effect refers to the stress redistribution and the failure-movement of the surrounding rocks because of the mining activities (Li and Cao 2005). The distribution of in situ stress is disturbed and the transmission of mining stress is blocked because of the fault occurrence. It is different from that of the general geological conditions.

In terms of the mining effect and dynamic phenomena with the fault occurrence, numerous studies have been conducted. Evolution of the mining-induced stress with the working face advancing towards a fault was studied by numerical simulation (Ji *et al.* 2012, Jiang *et al.* 2014). Characteristics of mining stress and fault activation were studied and analyzed when the working face advanced towards a fault with different mining-sequences (Jiang *et al.* 2015). The spatial-temporal laws of the normal stress and shear stress of the fault plane and the fault slipping laws were studied and revealed by Jiang *et al.* (2013). Dynamic numerical analysis was used, which revealed the maximum shear displacement affected by fault was related to the fault dip, mining depth, and its position relative to the coal seam mining. However, it had little effect on fault stiffness and dilation angle (Sainoki and Mitri 2014a). Barton's shear strength model was incorporated into the FLAC3D to analyze the potential effect of fault-slip bursts which revealed that the fault with rough surface might easily cause the larger seismic events than that of the smooth surface (Sainoki and Mitri 2014b). To conduct effective monitoring

∗Corresponding author, Ph.D. Student
E-mail: 15854848872@163.com
**Corresponding author, Ph.D.
E-mail: jlsh1989@ 126.com
[a]Professor
E-mail: jjqsd@163.com
[b]Ph.D.
E-mail: pqzheng_1231@163.com
[c]Ph.D. Student
E-mail: fengfan0213@126.com

http://www.techno-press.org/?journal=gae&subpage=7
ISSN: 2005-307X (Print), 2092-6219 (Online)

Fig. 1 On-site images after rock burst accidents

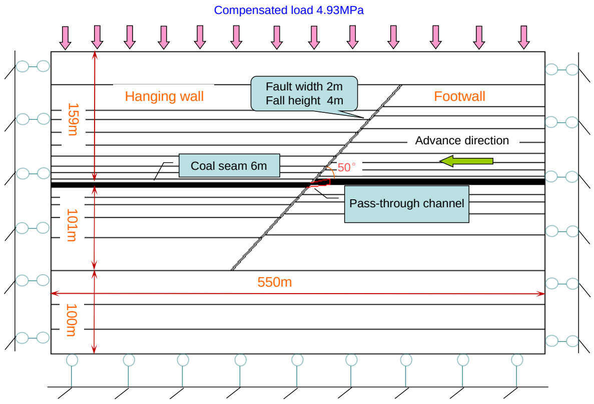

Fig. 2 Numerical calculation model

Table 1 Rock mass mechanical properties

Lithology	Density /kg·m^{-3}	Bulk/ GPa	Shear/ GPa	Cohesion/ MPa	Tensile strength /MPa	Internal friction angle/°
Siltstone	2530	8.82	4.84	3.30	2.47	30
Packsand	2530	7.87	3.38	3.26	2.19	28
Gritstone	2540	6.87	3.30	3.16	2.19	28
Mudstone	2340	2.17	1.00	1.30	1.15	38
Coal	1350	2.35	1.47	1.10	1.50	20
Fault	2000	1.55	1.25	0.001	0.40	30

and warning rock burst, the rock burst mechanism and the principle of using electromagnetic radiation from coal rock are studied by Song *et al.* (2017). The early warning signs of rock burst were studied and analyzed by different methods (Abdul-Wahed *et al.* 2006, Islam and Shinjo 2009, Jiang *et al.* 2010, Jiang *et al.* 2012,).

Previous studies have conducted considerable research on the characteristics of strata behaviors or the mechanical mechanism of fault slipping. However, the mining effect is often neglected. In addition, the systematic studies focusing on the mining effect and dynamic disasters with the working face advancing through a fault are few. Hence, the detailed research on the strata behaviors affected by a fault and fault stability induced by the mining activities with the working face advancing through the fault is further discussed.

Hence, according to the occurrence condition of a normal fault, the stress evolution of the working face and fault plane, the movement characteristics of overlying strata, and the law of fault slipping with the working face advancing from the footwall to the hanging wall are studied and analyzed utilizing UDEC numerical simulation. Further, the inducing-mechanism of fault rock burst is revealed. It might provide some important guiding for the prevention of the serious dynamic disasters, such as the outburst of coal and gas, the support of the roadway and roof control, and some other phenomena of mining pressure (Li *et al.* 2011, Zhang *et al.* 2013, Swift 2014, Rutqvist *et al.* 2015, Lei *et al.* 2015, Sainoki and Mitri 2015a, Li *et al.* 2016, Zhang *et al.* 2017).

2. Establishment of UDEC numerical model

The UDEC numerical simulation is a 2D discrete element program for non-continuous media. It also allows discrete blocks to have large deformation, sliding, and rotation along the joint surface. It has some advantages, such as less block division and fast operation speed comparing with the three-dimensional simulation software. It can simulate the stress and displacement of overlying strata clearly. Hence, the software can meet the actual needs of the study.

To meet the requirement of the study, a 550 m (length) × 366 m (high) model is established. Considering the boundary effect, the coal pillars with the width of 80 m are left on both sides of the model. Moreover, the floor strata with 201 m thickness in the hanging wall are maintained to eliminate the effect of bottom boundary on the stress state of the fault and the coal seam. Therein, the distance between the fault end and the bottom boundary is 100 m. The model can be divided in three parts including the hanging wall, the fault zone and the footwall as shown in Fig. 2. In the mine-wide model, meshes are discretized more densely around the coal where the stopes are extracted compared to the meshes in the areas near the model boundary. Thus, the discretization method makes it possible to simulate a stress state in the active mining areas as accurately as possible within the available computation capability (Sainoki and Mitri 2014c, 2015b, Hofmann and Scheepers 2015, Jiang *et al.* 2016, Jiang *et al.* 2017). In this study, the dip of the normal fault is the same as the advancing direction of the working face whose direction is from the footwall (right of the model) to the hanging wall (left of the model). The main characteristics of the model are as follows: thickness of coal seam 6 m, dip angle of normal fault 50°, fall height of the fault 4 m, and broken belt width of the fault 2 m.

Based on the field data, the rock masses are mostly made of mudstone, sandstone or other mixed sediments. Its physical and mechanical parameters are selected mainly based on rock mechanical tests. Due to the low strength of the fault zone, the parameters are appropriately weakened (Yi and Wang 2016). The rock mechanical parameters of the model are selected as shown in Table 1 (Su *et al.* 2002, Gao and Yang 2012, Jiang *et al.* 2015, Sainoki and Mitri 2015b, Zhang *et al.* 2015). The model uses the Mohr-Coulomb model to simulate the rock mass and follows the Mohr-Coulomb yield criterion, while the joint is calculated by the joint surface Contact-Coulomb slip model. According to Barton and Choubey (1977), the basic friction angle of a typical rock joint falls into a range of 21°-38° which is widely accepted by many researchers (Sainoki and Mitri 2014c, 2015b). Thus, in this study, the friction angle applied to the fault is considered 30°, which is an intermediate value in the range.

The full constraint boundary is used at the bottom of the calculation model, the left and right use the horizontal constraint boundary, and the top uses the free boundary. The simulated depth of coal seam is 356 m and the roof height of the model is 159 m, so the failed simulation of the overlying strata with the height of 197 m is presumed to be the vertical stress acting on the top of the model. Hence, the compensated load can be calculated by the Eq. (1) as follows

$$\sigma_v = \gamma h_v = 25\ \mathrm{kN \cdot m^{-3}} \times 197\mathrm{m} = 4.93\ \mathrm{MPa} \tag{1}$$

where γ and h_v are the unit weight of the rock mass and the height of the failed simulation strata. In the present study, the unit weight of the overlying rock mass is assumed to be 25 kN/m^3.

Considering the small fall height of the fault and based on relevant experience, the working face could pass through the fault directly because it can reduce the workload and improve the efficiency (Zhang and Chen 2013). Hence, we expect it to make an adjustment 15 m away from the fault and at an 8°-15° angle to the working face. Then the working face passes through the fault directly.

3. Evolution law of mining stress affected by normal fault

3.1 Characteristics of in situ stress affected by normal fault

The in situ stress of rock masses in a coalmine is related to its buried depth. In order to eliminate the effect of bottom boundary on in situ stress state, floor strata with 201 m in thickness have been built beneath the coal seam. Three monitoring lines of in situ stress which locate at the roof, coal seam and floor are set up, and the variation curves of the in situ stress at different layers are obtained as shown in Fig. 3(a). From Fig. 3(a), the monitoring stress of the coal seam and the floor in the non-fault-affected zone is about 9.11 MPa and 11.94 MPa which are basically same as the in situ stress calculated by self-weight stress. It indicates that the in situ stress state of coal seam and fault end is not affected by the bottom boundary in this model. Hence, the bottom boundary effect can be eliminated in this model.

However, because of the normal fault, the distribution of in situ stress varies and shows certain special characteristics as shown in Fig. 3(b). Hence, the results can be concluded as follows:

a. Because the continuity of strata is cut off by a fault, continuous transmission of the in situ stress is destroyed.

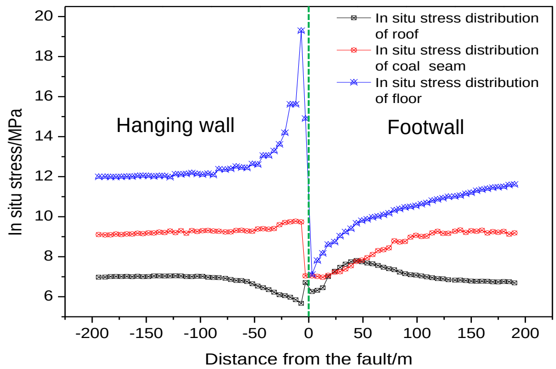

(a) Variation curves of in situ stress at different layers

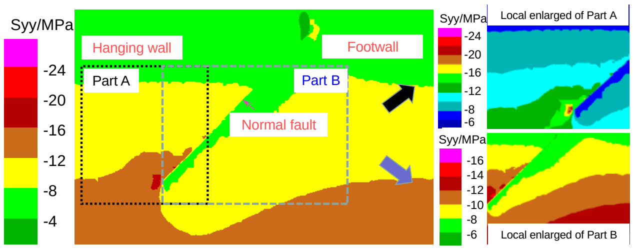

(b) Distribution nephogram of in situ stress

Fig. 3 In situ stress distribution

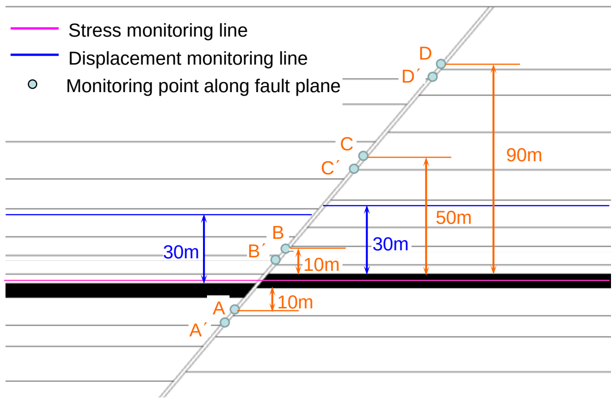

Fig. 4 Layout of the monitoring lines and points (local graph of model)

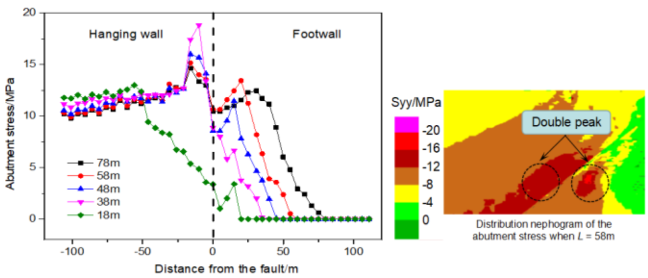

Fig. 5 Distribution of the abutment stress when the working face mines in the footwall

The difference between the two fault walls is much larger with increasing mining depth in the fault-affected zone as depicted in Fig. 3(a).

b. The in situ stress distribution of the two fault walls in fault-affected zone is notably different. The in situ stress concentrates highly near the fault end in the hanging wall. It expands in sector-shape away from the fault, as shown in

Part A of Fig. 3(b). Meanwhile, as the Part B of Fig. 3(b) shown that the distribution of in situ stress in the footwall is also affected by the fault, but the stress value barely varies. In addition, with the increasing of distance away from the fault, the in situ stress tends to be normal.

3.2 Mining stress evolution affected by normal fault

3.2.1 Evolution characteristics of mining stress in the footwall

A stress monitoring line is set up (as shown in Fig. 4) in the middle of the footwall coal seam. The evolution characteristics of abutment stress with the working face advancing towards the fault are analyzed as shown in Fig. 5.

It can be seen from Fig. 5 that when the working face in the footwall advances towards the fault, the distribution of the abutment stress shows a "double peak" pattern which is affected by the fault notably. The peak value of the abutment stress in the footwall decreases gradually with the fault coal pillar reduces; meanwhile that of in the hanging wall increases obviously.

When the distance between the working face and the fault is more than 58 m, namely $L \geq 58$ m, the peak value of the abutment stress increases gradually to 13.45 MPa and its affected range decreases because of the fault block. However, the stress value and its affected range in the hanging wall are negligible. When 38 m$>L>$18 m, the abutment stress in the footwall decreases obviously because of the fault coal pillar width decreasing. Moreover, the stress transfers towards the hanging wall and the abutment stress in the hanging wall increases notably to 18.83 MPa. When L=18 m, the abutment stress in the footwall rapidly decreases to 3.41 MPa due to severe damage of the fault coal pillar. Moreover, the bearing capacity of the hanging wall strata also decreases and the concentrated stress moves forward.

3.2.2 Distribution characteristics of mining stress as working face passes through the fault

According to the relevant experience, the working face passes through the fault at an angle of 8°-15° with breaking floor when L=15 m. During the progress of the working face passing through the fault, the mining-induced failure of rocks would link up with the fault zone which may cause fault instability. Moreover, the cantilever rocks of hanging wall would rotate towards the fault direction and deforms because the constraint ability of the footwall to the hanging wall decreases. Hence, the peak value of the abutment stress in hanging wall increases obviously to 13.73 MPa because of the effect of the suspended rocks in hanging wall, as shown in Fig. 6.

In addition, because of the fault cutting and the weak strength of fault zone, the surrounding rocks are prone to failure-movement and the floor might heave. Hence, the support of the working face and the roadway should be enhanced during the progress of the working face passing through the fault.

3.2.3 Evolution characteristic of mining stress in the hanging wall

When the working face passes through the fault and the distance between the working face and the fault is 7 m, it can be named L=-7 m. At present, the abutment stress in the hanging wall has little variation with the pervious mining and the peak value is 13.71 MPa. As the working face advances towards to the fault for 17 m (L=-17 m), the abutment stress in the hanging wall concentrates higher due to the suspension of roof rocks. The peak value of the abutment stress rises notably to 15.03 MPa. When L<-17 m, the distribution of the abutment stress tends to normal and the effect caused by the fault weakens gradually. Moreover, the abutment stress moves forward and the values have not much of a change.

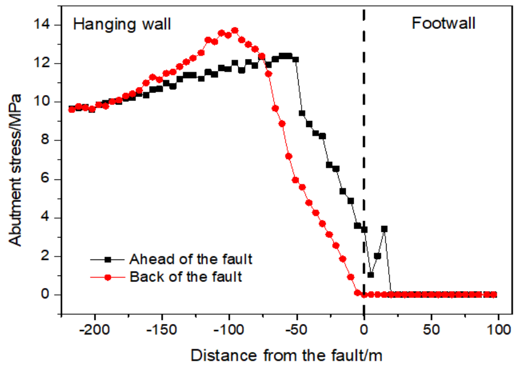

Fig. 6 Variation of the abutment stress during the progress of the working face passing through the fault

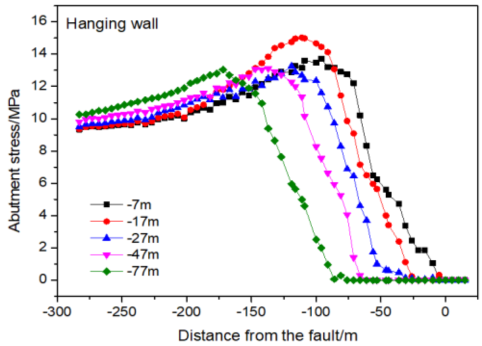

Fig. 7 Distribution of the abutment stress after the working face passing through the fault

4. Stress evolution law of fault plane

4.1 Evolution of normal stress at fault plane

Several stress monitoring points are set up along the fault plane with different layers as shown in Fig. 4, including the floor, immediate roof, main roof, and high-position layer. The points are at a distance of -10 m, +10 m, +50 m, and +90 m ("+" means the point is over the coal seam), respectively, from the coal seam. The monitoring points are named A, B, C and D which are in the footwall and A', B', C', and D' which are in the hanging wall. Hence, the evolution of fault plane stress is shown in Figs. 8 and 9.

As can be seen from Fig. 8, the normal stress variation of the monitoring points in footwall and hanging wall is similar. When $L \leq 28$ m, the normal stress of point A at the floor is relatively small which is caused by the mining disturbance. Points B and C at the roof are in the stress-

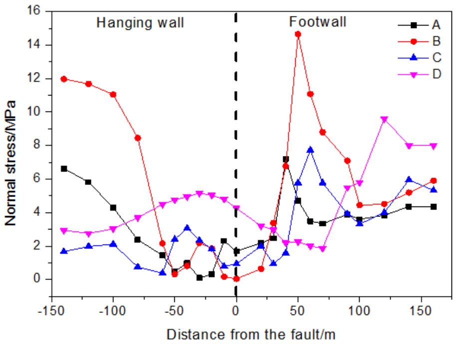

(a) Monitoring foot points in foot wall

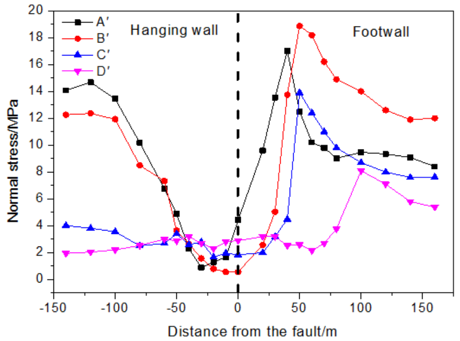

(b) Monitoring foot points in hanging wall

Fig. 8 Variation of the normal stress at the fault plane

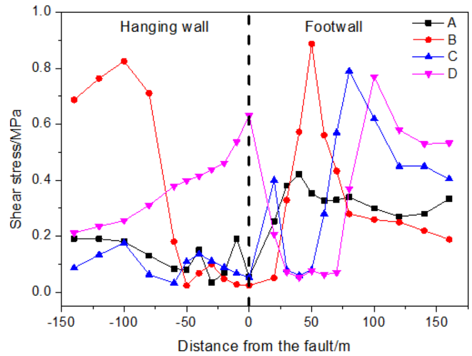

(a) Monitoring foot points in foot wall

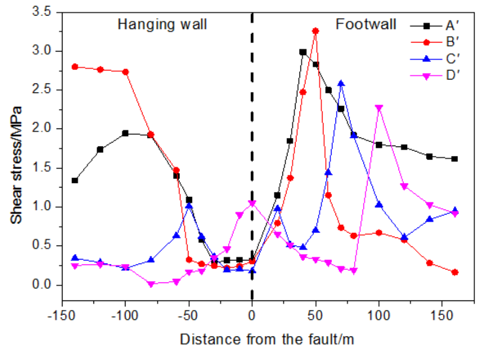

(b) Monitoring foot points in hanging wall

Fig. 9 Variation of the shear stress at the fault plane

relief state with small normal stress when -17 m≤L≤38 m. The normal stress of point D at the high-position layer varies easier than the other three points because it began varying at 98 m. In addition, according the two diagrams of the Figs. 8(a) and 8(b), the variations of monitoring points in the hanging wall are slightly delayed from that of the footwall because of fault cutting.

Hence, it can be concluded that the normal stress at the fault plane varies from the higher layer to the lower one subsequently. The high-position layer is affected primarily and the stress decreases with the large distance between the working face and the fault. Then, the main roof and the immediate roof enter a stress-relief state during the working face passing through the fault. Finally, the floor de-stresses which is caused by the mining disturbance.

In Fig. 9, we can see that the shear stress of point A at the floor decreases after L=28 m; then it varies slightly and shows oscillation. Meanwhile the normal stress decreases which indicates the floor fault has intermittent slipping (Wang 2012). Both the shear stress and the normal stress of point B increase with 28 m≤L≤98 m. However, the increasing amplitude of the former is larger than the latter. When L=78 m, the shear stress of point C increases notably and the normal stress decreases. It might represent that it has a large slipping risk. Then, as the working face advances towards the 18m away from the fault, the shear stress increases again and the possibility of the fault slipping is also larger. Both the normal stress and shear stress of point D are affected primarily and then the shear stress increase rapidly at L=0 m. Hence, it can be seen that the point D has larger slipping risk with the two positions of L=0 m and L=98 m. Additional, the shear stress variation of the monitoring points in the hanging wall is larger than that of the footwall.

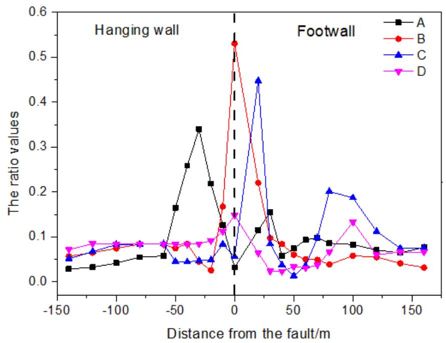

(a) Monitoring foot points in foot wall

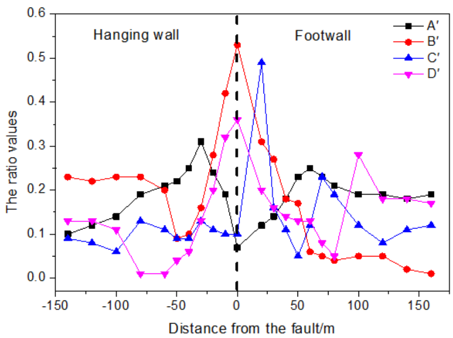

(b) Monitoring foot points in hanging wall

Fig. 10 Variation of the ratio of shear stress to normal stress

4.2 Risk analysis of the fault slipping

Fault activation and slipping depends on the relationship between the normal stress and the shear stress. A separate study on either of both stresses cannot directly reflect the risk (Li *et al.* 2008, Jiang *et al.* 2013, 2015). Hence, the ratio of shear stress to normal stress could be used as the indicator for the fault activation and slipping as shown in Fig. 10.

As can be seen from Fig. 10, the ratio of shear stress to normal stress of point A at the floor is small when $L \geq 38$ m. Then, two peak values with 0.15 and 0.34 are occurred which positions correspond to L=28 and L=-27 m, respectively. It indicates that the floor fault has the risk possibly of fault slipping near the two positions. When 0 m≤L≤28 m, the ratio values of point B increase rapidly and the maximum value is 0.53 with L=0 m. It means the risk of fault slipping is larger during the progress of the working face passing through the fault. The ratio of point C also has two peak values at the positions of L=78 m and L=18 m. However, the latter value of 0.45 is great than the former value of 0.20 which indicates that the risk of fault slipping with L=18 m is larger than that of L=78 m. The fault slipping risk of point D might show around the 98 m and 0 m because of the ratio values of the two positions are large.

Hence, it can be seen that the risk of fault slipping in the affected zone with the larger ratio values is higher. Moreover, it has obvious spatial and temporal characteristics due to the occurrence of fault slipping from the higher layer to the lower one in sequence.

5. Evolution laws of roof subsidence and fault slipping

5.1 Evolution laws of roof subsidence

Two displacement monitoring lines are set up in the roof with 30 m above the coal seam as shown in Fig. 4, and the subsidence curve is obtained in Fig. 11.

As can be seen from Fig. 11, when L > 38 m, the deformation range and subsidence value of overlying strata in the footwall increase while that of the hanging wall has not much of a change. The curve distributes in a V-shape and the valley value moves forwards gradually. Then the roof failure-movement spreads to the fault zone when 18 m≤L≤38 m and the roof subsidence between the working face and the fault increases notably because of the fault cutting. The maximum value rises to 3.91 m when L=18 m. Meanwhile, the hanging wall strata rotate towards the fault direction because of the bearing ability decreasing of the footwall strata. With the working face advancing further, the local strata in the footwall move and subsidence values increase. However, the hanging wall strata continue to rotate and move which would result in the increasing of subsidence value. Then, the subsidence curve extends to a U-shape instead of the V-shape.

5.2 Subsidence curves of rocks at both sides of fault

Four adjacent displacement monitoring points (marked as a, b, c and d) on the fault plane, which are located on the same layers with the A, B, C and D, respectively, are set up to understand the movement laws of the strata at the both sides of the fault.

From Fig. 12, the floor strata have heave deformation and an incompatible deformation of two fault walls exists

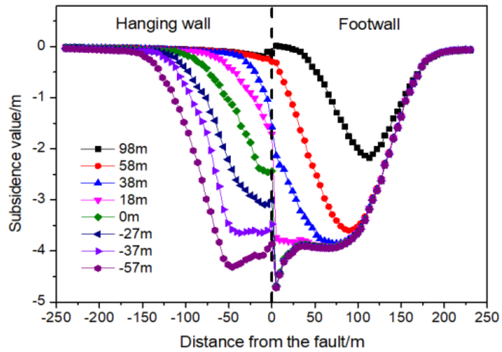

Fig. 11 Subsidence curves of roof

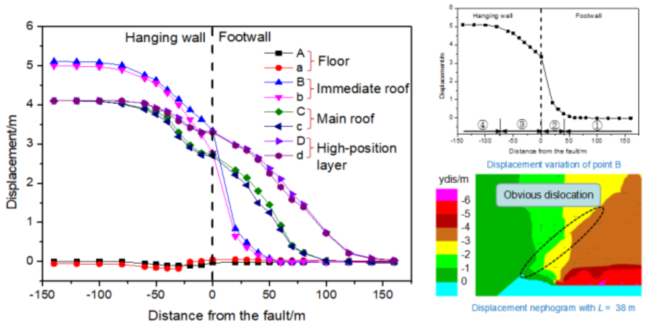

Fig. 12 Subsidence curves of rocks at both sides of fault

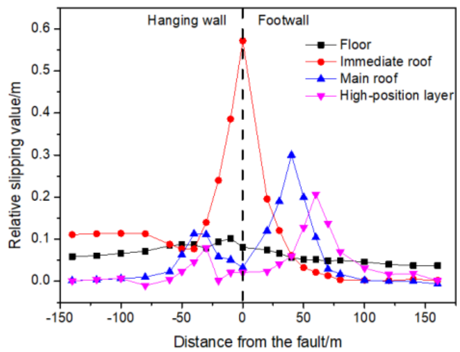

Fig. 13 Relative slipping along fault plane

when the working face mines in the hanging wall. The variation of the roof subsidence distributes in S-shape, which successively experiences four stages of (1) slow deformation, (2) violent slipping, (3) deformation induced by the hanging wall strata rotation, and (4) movement stability. Moreover, the deformation begins from the higher layers to the lower ones. However, even though the deformation curves of the two fault walls in the same layers are similar, an incompatible deformation is existed which could represent the activation and slipping of the roof fault.

In Fig. 12, the slope of the subsidence curve represents the subsidence rate of the roof. When the working face advances towards the fault, the subsidence rate increases notably. It indicates the fault activates and a large amount of strain energy releases violently (Wang 2012). Hence, it might interpret why the fault rock burst easily occurs in the footwall during the working face advances through the fault.

5.3 Analysis of the relative slipping of fault

In Fig. 13, the variation of relative slipping of floor fault is small and the values are relatively stable; while that of the roof fault distributes in a notable “single peak” and the peak value increases gradually from the higher layer of 0.21 m to the lower layer of 0.57 m. The relative slipping value of the high-position layer begins to increase at L=98 m firstly and rises to maximum of 0.21 m when L=58 m. The main roof and immediate roof begin to move at L=78 m and 48 m. Moreover, the relative slipping values rise to maximum of 0.30 m and 0.57 m when L=38 m and 0 m. Hence, the fault activation at the higher layer is earlier than that at the lower layer because of the fault dip same with the advancing direction of the working face.

Hence, from the analysis of the sections 4 and 5, it can be concluded that as the working face advances, the two fault walls loose and the adhesive capacity reduces affected by the mining activities. Then, the normal stress of fault plane decreases and the shear stress increases relatively which might induce the fault activation and slipping, thereby easily inducing the fault rock burst.

6. Discussion in causes of rock burst affected by fault

Mining activities lead to the stress redistribution and the mining-induced stress concentrates highly in the vicinity of the fault because of the fault cutting. Meanwhile, it affects the fault plane and results in the local deformation which could cause the stress and the strain energy of surrounding rocks increase notably. The shear stress of fault plane would rise and violent slipping might occur when the sufficient strain energy is accumulated along the fault due to large asperities or bridges between fractures which might easily induce the fault rock burst (Li 2009, Sainoki and Mitri 2014c, Li *et al.* 2016).

Hence, the relationship among the mining activities, fault activation and fault rock burst is shown in Fig. 14.

On-site experience shows that the fault rock burst is more easily induced in the vicinity of the fault in which more strain energy is released and violent destruction might be caused. For instance, an accident of the rock burst affected by the fault marked as SF28 occurs in the tailgate of 6303 working face in Jining No.3 coalmine when the distance between the working face and the normal fault is 66m; a coal body outburst instantaneously along with the tremendous sound and the devices are overturned. A shock bump affected by the fault marked as XF-20 occurs in the $103_{upper}02$ working face in a Baodian coalmine which results in the strong tremor in the working face and its roadway. Hence, the simulation results reveal the mechanism of rock burst with the occurrence of a fault. Moreover, it can provide a scientific basis for safe mining under similar geological conditions.

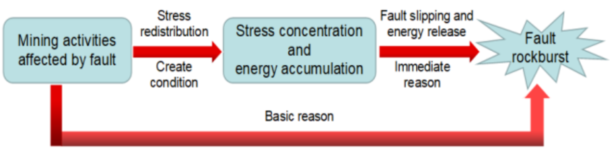

Fig. 14 Relationship among the mining activities, fault activation and fault rock burst

7. Conclusions

In this paper, the stress evolution of the working face and fault plane, the movement characteristics of overlying strata, and the law of fault slipping with the working face advancing from the footwall to the hanging wall are conducted in order to investigate the effect of the normal fault on the rock burst. A numerical model was generated by means of UDEC software.

It can be concluded that in pre-mining, the in situ stress distribution of the two fault walls is notably different. Moreover, the difference is much larger with increasing mining depth in the fault-affected zone. When the working face mines in the footwall, the abutment stress distributes in a “double peak” pattern. The ratio of shear stress to normal stress of fault plane has the obvious spatial and temporal characteristics because it varies gradually from the higher layer to the lower one orderly. The variation of roof subsidence is in S-shape. It successively experiences four stages, including slow deformation, violent slipping, deformation induced by the hanging wall strata rotation, and movement stability. Moreover, the deformation also begins from the higher layers to the lower ones. The roof relative slipping of two fault walls distributes in “single peak”, and the peak value increases from the high-position layer to the immediate roof. Finally, some field cases of the fault rock burst or shock bump are used to verify the numerical simulation results.

The results utilized for studying the mining effect influenced by the normal fault have great significance concerning the prediction and prevention of the fault rock burst.

Acknowledgments

The research described in this paper was financially supported by the National Natural Science Foundation of China (51574155), Tai'an Science and Technology Development Plan of Shandong Province (2015ZC1058), Science and Technology Innovation Fund of College of the Mining and Safety Engineering, Shandong University of Science and Technology (KYKC17008), and State Key Laboratory for GeoMechanics and Deep Underground Engineering, China University of Mining & Technology (SKLGDUEK1725), and research funding from Government of Shandong Province (J17KA212).

References

Abdul-Wahed, M.K., Heib, M.A. and Senfaute, G. (2006), “Mining-induced seismicity: Seismic measurement using multiplet approach and numerical modeling”, *J. Coal. Geol.*, **66**(1), 137-147.

Barton, N. and Choubey, V. (1977), “The shear strength of rock joints in theory and practice”, *Rock Mech*., **10**(1-2), 1-54.

Fan, C.J., Li, S., Luo, M.K., Du, W.Z. and Yang, Z.H. (2017), “Coal and gas outburst dynamic system”, *J. Min. Sci. Technol*., **27**(1), 49-55.

Gao, R. and Yang, L.Q. (2012), *Analysis of Rock Slope Stability Using Anti-Slide Pile*, in *Advanced Material Research*, Trans

Tech. Publications, 2470-2473.

Hofmann, G.F. and Scheepers, L.J. (2015), “Simulating fault slip areas of mining induced seismic tremors using static boundary element numerical modeling”, *Trans. Inst. Min. Metall. Sect. A*, **120**(1), 53-64.

Islam, M.R. and Shinjo, R. (2009), “Mining-induced fault reactivation associated with the main conveyor belt roadway and safety of the Barapukuria coal mine in Bangladesh: Constraints from BEM simulations”, *J. Coal. Geol.*, **79**(4), 115-130.

Ji, H.G., Ma, H.S., Wang, J.A., Zhang, Y.H. and Cao, H. (2012), “Mining disturbance effect and mining arrangements analysis of near-fault mining in high tectonic stress region”, *Safety Sci.*, **50**(4), 649-654.

Jiang, F.X., Miao, X.H., Wang, C.W., Song, J.H., Deng, J.M. and Meng, F. (2010), “Predicting research and practice of tectonic-controlled coal burst by microseismic monitoring”, *J. Chin. Coal. Soc.*, **35**(6), 900-903.

Jiang, J.Q., Wu, Q.L. and Qu, H. (2014), “Evolutionary characteristics of mining stress near the hard-thick overburden normal faults”, *J. Min. Safety Eng.*, **31**(6), 881-887.

Jiang, J.Q., Wu, Q.L. and Qu, H. (2015), “Characteristic of mining stress evolution and activation of the reverse fault below the hard-thick strata”, *J. Chin. Coal. Soc.*, **40**(2), 267-277.

Jiang, L.S., Sainoki, A., Mitri, H.S., Ma, N.J., Liu, H.T. and Hao, Z. (2016), “Influence of fracture-induced weakening on coal mine gateroad stability”, *J. Rock Mech. Min. Sci.*, **88**, 307-317.

Jiang, L.S., Wang, P., Zhang, P.P., Zheng, P.Q. and Xu, B. (2017), “Numerical analysis of the effects induced by normal faults and dip angles on rock bursts”, *Comtes Renuds Mecanique*, **345**(10), 690-705.

Jiang, Y.D., Lv, Y.K., Zhao, Y.X. and Cui, Z.J. (2012), “Principal component analysis on electromagnetic radiation rules while fully mechanized coal face passing through fault”, *Proc. Environ. Sci.*, **12**, 751-757.

Jiang, Y.D., Wang, T., Zhao, Y.X. and Wang, C. (2013), “Numerical simulation of fault activation pattern induced by coal extraction”, *J. Chin. Univ. Min. Technol.*, **42**(1), 1-5.

Lei, D.J., Li, H. and Meng, H. (2015), “Geological division of gas in the Pingdingshan mine area based on its tectonic dynamics characteristics”, *J. Min. Sci. Technol.*, **25**(5), 827-833.

Li, J.P. and Cao, P. (2005), “Catastrophe analysis on pillar instability considered mining effect”, *J. Central South Univ. Technol.*, **12**(1), 102-106.

Li, L.C., Yang, T.H., Liang, Z.Z., Zhu, W.C. and Tang, C.A. (2011), “Numerical investigation of groundwater outbursts near faults in underground coal mines”, *J. Coal Geol.*, **85**(3-4), 276-288.

Li, T., Mu, Z.L., Liu, G.J., Du, J.L. and Lu, H. (2016), “Stress spatial evolution law and rockburst danger induced by coal mining in fault zone”, *J. Min. Sci. Technol.*, **26**(3), 409-415.

Li, X.H., Pan, F., Li, H.Z., Zhao, M., Ding, L.X. and Zhang, W.X. (2016), “Prediction of rock-burst-threatened areas in an island coal face and its prevention: A case study” *J. Min. Sci. Technol.*, **26**(6), 1125-1133.

Li, Z.H. (2009), “Research on rock burst mechanism induced by fault slip during coal mining operation”, Ph.D. Dissertation, China University of Mining and Technology, Xuzhou, China.

Li, Z.H., Dou, L.M., Lu, C.P., Mu, Z.L. and Cao, A.Y. (2008), “Study on fault induced rock bursts”, *J. Min. Sci. Technol.*, **18**(3), 321-426.

Rutqvist, J., Rinaldi, A.P., Cappa, F. and Moridis, G.J. (2015), “Modeling of fault activation and seismicity by injection directly into a fault zone associated with hydraulic fracturing of shale-gas reservoirs”, *J. Petrol. Sci. Eng.*, **127**, 377-386.

Sainoki, A. and Hani, S.M. (2014a), “Dynamic behaviour of mining-induced fault slip”, *J. Rock Mech. Min. Sci.*, **66**(1), 19-29.

Sainoki, A. and Hani, S.M. (2014b), “Dynamic modelling of fault-slip with Barton's shear strength model”, *J. Rock Mech. Min. Sci.*, **67**, 155-163.

Sainoki, A. and Hani, S.M. (2014c), “Methodology for the interpretation of fault-slip seismicity in a weak shear zone”, *J. Appl. Geophys.*, **110**, 126-134.

Sainoki, A. and Hani, S.M. (2015a), “Effect of slip-weakening distance on selected seismic source parameters of mining-induced fault-slip”, *J. Rock Mech. Min. Sci.*, **73**, 115-122.

Sainoki, A. and Hani, S.M. (2015b), “Evaluation of fault-slip potential due to shearing of fault asperities”, *Can. Geotech. J.*, **52**(10), 1417-1425.

Song, D.Z., Wang, E.Y., Li, Z.H., Qiu, L.M. and Xu, Z.Y. (2017), “EMR: An effective method for monitoring and warning of rock burst hazard”, *Geomech. Eng.*, **12**(1), 53-69.

Su, S.R., Zhu, H.H., Wang, S.T. and Stephansson, O. (2002), “The effect of fracture properties on stress field in the vicinity of a fracture”, *J. Northwest Univ.*, **32**(6), 655-658.

Swift, G. (2014), “Relationship between joint movement and mining subsidence”, *Bull. Eng. Geol. Environ.*, **73**(1), 163-176.

Wang, T. (2012), “Mechanism of coal bumps induced by fault reactivation”, Ph.D. Dissertation, China University of Mining and Technology, Xuzhou, China.

Wang, Y. (2010), “Discrete Element Analysis on the water Proof Pillar to coal seam mining goaf beside large fault”, Ph.D. Dissertation, Hefei University of Technology, Hefei, China.

Yi, W.X. and Wang, E.Y. (2016), “Experimental research on measurement of permeability coefficient on the fault zone under coal mine in situ”, *Arab. J. Geosci.*, **9**(4), 1-9.

Yong, Y., Tu, S.H., Zhang, X.G. and Li, B. (2015), “Dynamic effect and control of key strata break of immediate roof in fully mechanized mining with large mining height”, *Shock. Vibr.*, **2015**, 1-11.

Zhang, C.Q., Feng, X.T., Zhou, H., Qiu, S.L. and Wu, W.P. (2013), “Rockmass damage development following two extremely intense rockbursts in deep tunnels at Jinping II hydropower station, southwestern China”, *Bull. Eng. Geol. Environ.*, **72**(2), 237-247.

Zhang, D.F. and Chen, Y. (2013), “Research and application of roof activity regulation when fully-mechanized caving face passing through fault”, *China Coal*, **39**(4), 56-59.

Zhang, J., Li, S.C., Li, L.P., Zhang, Q.Q., Xu, Z.H., Wu, J. and He, P. (2017), “Grouting effects evaluation of water-rich faults and its engineering application in Qingdao Jiaozhou Bay Subsea Tunnel, China”, *Geomech. Eng.*, **12**(1), 35-52.

Zhang, Y.T., Ding, X.L., Pei, Q.T. and Zhang, Z.G. (2015) “Modelling mechanical response of geological fault structures and their interaction analysis with surrounding rock”, *Open Civ. Eng. J.*, **9**(1), 471-476.

CC